Sterilization of granulomas is common in both active and latent tuberculosis despite extensive within-host variability in bacterial killing

Published in final edited form as:
Nat Med. 2014 January ; 20(1): 75–79. doi:10.1038/nm.3412.

Sterilization of granulomas is common in both active and latent tuberculosis despite extensive within-host variability in bacterial killing

Philana Ling Lin[1,*], **Christopher B. Ford**[2,3,*], **M. Teresa Coleman**[4], **Amy J. Myers**[5], **Richa Gawande**[2], **Thomas Ioerger**[6], **James Sacchettini**[7], **Sarah M. Fortune**[2,3,8,§], and **JoAnne L. Flynn**[5,§]

[1]Department of Pediatrics, Children's Hospital of Pittsburgh of the University of Pittsburgh Medical Center, Pittsburgh, Pennsylvania, USA.

[2]Department of Immunology and Infectious Diseases, Harvard School of Public Health, Boston, Massachusetts, USA.

[3]Broad Institute of MIT and Harvard, Cambridge, Massachusetts, USA.

[4]Department of Radiology, PET Center, University of Pittsburgh School of Medicine, Pittsburgh, Pennsylvania, USA

[5]Department of Microbiology and Molecular Genetics, University of Pittsburgh School of Medicine, Pittsburgh, Pennsylvania, USA.

[6]Department of Computer Science and Engineering, Texas A&M University, College Station, Texas, USA.

[7]Department of Biochemistry and Biophysics, Texas A&M University, College Station, Texas, USA.

[8]Ragon Institute of MGH, MIT, and Harvard, Boston, Massachusetts, USA.

Abstract

Over 30% of the world's population is infected with *Mycobacterium tuberculosis* (Mtb), yet only ~5–10% will develop clinical disease[1]. Despite considerable effort, we understand little about what distinguishes individuals who progress to active tuberculosis (TB) from those who remain latent for decades. The variable course of disease is recapitulated in cynomolgus macaques infected with Mtb[2]. Active disease in macaques is defined by clinical, microbiologic and immunologic signs and occurs in ~45% of animals, while the remaining are clinically asymptomatic[2,3]. Here, we use barcoded Mtb isolates and quantitative measures of culturable and cumulative bacterial burden to show that most lesions are likely founded by a single bacterium and reach similar maximum burdens. Despite common origins, the fate of individual lesions varies substantially within the same host. Strikingly, in active disease, the host sterilizes some lesions

[§]Corresponding author, SMF: sfortune@hsph.harvard.edu, JLF: joanne@pitt.edu.
[*]These authors contributed equally to this work

Author Contributions.
P.L.L., C.B.F., S.M.F., and J.L.F. conducted experiments, analyzed results, and drafted the manuscript. R.G., T.I. and J.S. performed Illumina sequencing and edited the manuscript. M.T.C. performed PET-CT analysis and assisted necropsies. A.J.M. conducted experiments.

Competing Financial Interests.
The authors declare no competing financial interests.

even while others progress. Our data suggest that lesional heterogeneity arises, in part, through differential killing of bacteria after the onset of adaptive immunity. Thus, individual lesions follow diverse and overlapping trajectories, suggesting critical responses occur at a lesional level to ultimately determine the clinical outcome of infection. Defining the local factors that dictate outcome will be important in developing effective interventions to prevent active TB.

A prevailing model in the TB field is that the immune response in individuals that progress to active disease is less effective than the response in individuals that develop a latent infection. This model suggests that most lesions will behave similarly within a given individual in response to the systemic immune response, and that global differences in lesional dynamics between individuals ultimately result in different clinical outcomes. However, recent studies suggest this view is overly simplistic [2,4–8]. Using ^{18}F-fluorodeoxyglucose (FDG) with positron emission tomography and computed tomography (PET-CT) imaging, we find that the metabolic activity (measured as standard uptake volume ratio, SUVR) of individual lesions is independent and dynamic during infection, even within the same host (Fig. 1a). The SUVR of each lesion loosely correlates with CFU (Spearman's • = 0.4431, $p < 0.0001$) (Fig. 1b), suggesting lesional variability in both host response and bacterial growth. We also find a wide spectrum of lesion types by histopathology within individual animals[2], similar to descriptions of lesions in TB patients in the preantibiotic era[9]. These findings together appear inconsistent with the idea of a host response that is globally restrictive or permissive[2,10].

We therefore sought to define the quantitative dynamics of lesion formation and progression. To understand the initial formation of multiple sites of infection, we leveraged a sequenced panel of eight Mtb isolates, each distinguished by a single nucleotide polymorphism (SNP)[11], creating a molecular barcode for each isolate (Supplemental Table 1). We find no evidence that the individual SNPs altered bacterial fitness *in vitro* (Supplemental Fig. 1a). We infected two macaques with a small dose (~34 CFU) of this inoculum and followed individual lesions temporally by PET-CT. After 4 weeks, animals were necropsied, and we quantified the relative abundance of each barcode in individual granulomas by amplicon deep sequencing. The median CFU per lesion for these animals is similar to the median CFU per lesion at 4 weeks in animals infected with wild type Mtb Erdman (Supplemental Fig. 1b).

Though all eight barcodes were represented in each animal, strikingly, 79% of individual granulomas contained only one barcode. There are two possible explanations for these data. Either most granulomas are only founded by a single bacterium (Fig. 2a, Supplemental Table 2), or in each granuloma, a single isolate outcompeted the others. If fitness differences were responsible for these observations, then the prevalence of more fit isolates should increase significantly from their prevalence in the inoculum. We developed a stochastic mathematical simulation to predict the prevalence of each barcoded isolate *in vivo* based on random sampling from the stock to generate the inoculum (Supplemental Fig. 1c,d). No isolates were significantly underrepresented *in vivo*, but one barcode, I3, was significantly overrepresented after 4 weeks ($p = 0.023$), consistent with a 1% increase in fitness (Supplemental Fig. 1d,e). However, after removing all lesions containing I3 from our analysis (excluding seven of 45 lesions), 88% of lesions still contain only one barcode. Thus, our data suggest that most granulomas arise from an individual bacterium.

In most lesions where more than one barcode was identified, there was histologic evidence of multi-focal lesions (data not shown). Yet even among multi-focal lesions, 64% contained a single barcode, suggesting the majority arose via localized spreading as opposed to coalescence of nearby lesions. In contrast, thoracic lymph nodes often contained several different barcodes (Fig. 2a). There was no significant correlation between bacterial burden

and the number of founder bacteria in individual lesions (Fig. 2b) although lesions arising at earlier time points had a significantly higher burden (~6 fold, $p = 0.0012$) than lesions arising 1 – 2 weeks later (Fig. 2c).

We next sought to assess the trajectory of the bacterial population in individual lesions from 4 –11 weeks post infection, coinciding with the onset of the adaptive immune response. We infected seven macaques, tracked lesions using FDG PET – CT, and then measured CFU/lesion. At 4 weeks, the median bacterial burden in individual granulomas was ~1.8×10^4 CFU (Fig. 3a), but was reduced significantly (~15 fold, $p = 0.0002$) by 11 weeks, suggesting significant killing after the onset of adaptive immunity. Though it is too early to distinguish latent and active disease at 11 weeks, one animal had a significantly higher median bacterial burden than the other two, suggesting an inflection point in disease trajectory (Fig. 3b, $p < 0.05$). However, there was also a striking range of bacterial burdens ($10^2 – 10^6$ CFU per lesion) within each macaque, suggesting that the extent of killing varies dramatically between lesions.

To understand how these early phenotypes relate to disease outcome, we next assessed bacterial burden in lesions from animals with active disease or latent infection. While animals with active TB harbor significantly more bacteria than animals with latent infection[2], at a lesional level there is a broad and overlapping distribution of CFU per granuloma (Fig. 3a, Supplemental Fig. 2a,b). Importantly, the median CFU of individual lesions from animals with active disease and latent infection is ten to 100 fold lower than lesions in animals at 4 and 11 weeks post–infection (Fig. 3a) and a substantial number of lesions in animals with active disease and latent infection are sterile (no CFU were cultured after 6 weeks on solid medium) (Fig. 3c). While we cannot rule out the possibility of viable but nonculturable bacteria in these sterile lesions, we have previously shown that lesional CFU do not significantly increase after extended culture (~1 year)[2]. Moreover, while immunosuppression should allow reactivation of quiescent Mtb, latent animals treated with anti–TNF antibody[10,12] contain a similar proportion of sterile lesions (54%) as untreated latent animals (58%).

The comparison of lesional CFU suggests that the efficacy of bacterial killing dictates lesional bacterial burden and that there is marked lesion–to–lesion variability in bacterial killing. To test this model, we took advantage of the finding that genomes (chromosomal equivalents, CEQ) from nonviable Mtb are not degraded but instead persist in tissues in the mouse model of TB[13]. The number of genomes reflects the cumulative bacterial burden and the ratio of CFU to CEQ reflects the degree of killing. To determine whether genomes of killed Mtb are similarly stable in macaque lesions, we compared CEQ from animals treated with two months of isoniazid (INH) to CEQ from untreated animals over a similar time frame (Supplemental Fig. 2c). Median CEQ in lesions from treated animals were orders of magnitude higher than CFU, though only ~20 fold lower than CEQ in lesions from untreated animals. We conclude that while genomes may degrade slowly over time in macaque lesions, the rate of decay is slow enough that CEQ can be used to estimate cumulative bacterial burdens per lesion across animals.

We assessed CEQ in lesions from animals at 4 and 11 weeks p.i. and from those with active disease and latent infection. Strikingly, CEQ were stable across disease states, and CEQ from sterile lesions are indistinguishable from CEQ from non–sterile lesions (Fig. 3d). The only significant difference in CEQ was between 4 week and active animals (actives ~3.5 fold greater than 4 weeks, $p < 0.01$), though the number of viable bacteria in lesions (CFU) from every group of animals was significantly different (Fig. 3a, $p < 0.001$). CFU/CEQ reflects the proportion of the bacterial population that is still viable, having not been killed. There was minimal killing at 4 weeks but by 11 weeks, CFU/CEQ was significantly reduced

compared to 4 weeks, and even lower in animals with active and latent infection (Fig. 3e, $p < 0.001$). Thus, as the adaptive immune response is induced, killing of bacteria in individual lesions occurs, even to the point of lesional sterilization. Furthermore, both animals with latent infection and active disease have the capacity to sterilize lesions, demonstrating that the capacity to sterilize a lesion is not a hallmark of latent infection alone.

To estimate the rate of Mtb growth and killing in lesions, we developed and fit an ordinary differential equation based logistic model of bacterial dynamics in the host (Fig. 4a, Supplemental Table 3, Supplemental Fig. 3). Our data are best fit by a model in which there is an initial rapid growth phase after which bacterial growth is drastically slowed, and bacterial death leads to a reduction in CFU. Our CEQ data suggest that lesions reach a maximum bacterial burden or "carrying capacity" coincident with the onset of adaptive immunity. Carrying capacity is likely driven by multiple factors, including the immune response and the maximum physical capacity of a granuloma, where lesions that progress beyond this capacity may spread locally or lead to TB pneumonia[2]. Indeed, measuring CFU and CEQ per gram in regions of TB pneumonia from animals with active disease, we find no evidence of bacterial killing (median CFU/CEQ = 1.05), suggesting that these sites are permissive environments for *Mtb* survival (Fig. 4b,c).

These data suggest that the histopathology of a lesion may predict local killing capacity. We sought to define the associations between histopathology, time after infection, and CFU/CEQ (Fig. 4d). A correlation matrix reveals that TB pneumonia is positively correlated with CFU/CEQ ($r = 0.66$, $p = 9.24E{-}07$), and poorly correlated with time post infection, suggesting that at any time in infection, there is little killing in areas of TB pneumonia. By excluding TB pneumonia samples, we find that fibrocalcific lesions are negatively correlated with CFU/CEQ ($r = -0.56$, $p = 0.002$) and represent sites of bacterial control; whereas caseous sites are associated with poor control ($r = 0.4376$, $p = 0.0086$) (Fig. 4e). However, both fibrocalcific and caseous lesions are significantly correlated with time post-infection ($r = 0.8016$ and -0.7350; $p = 7.189e\text{-}9$ and $4.957e\text{-}7$, respectively), suggesting that over time, killing increases and the dominant lesion type switches from caseous to fibrocalcific. These data are consistent with our previous findings in which animals with active TB were treated with short course anti-tuberculous treatment. Residual bacterial growth after treatment occurred primarily in caseous granulomas and TB pneumonia[10].

Ultimately, these data imply that the difference in bacterial numbers is driven largely by killing efficacy, which varies significantly among lesions even within a single animal. Animals with active disease and latent infection have similar capacity for bacterial killing in individual lesions (Fig. 3f). However, animals with active disease can simultaneously have sites of extensive tissue pathology (i.e. TB pneumonia) where there is little bacterial killing. Given this heterogeneity, it is not surprising that relevant predictors of disease outcome have been hard to identify from peripheral measures of immune response[14,15]. As virtually all macaques appear capable of eliminating infection at the lesional level, defining the mechanism of lesion sterilization may provide a path to a TB vaccine capable of generating sterilizing immunity.

Methods

Macaque infection and clinical classification

Healthy adult (>4 years, males) cynomolgus macaques (*Macacca fasicularis*) (Valley Biosystems, Sacramento, CA) were infected via bronchoscopic instillation of low dose (~25 CFU) *M. tuberculosis* (Erdman strain) as previously described [2,3] (Supplemental Table 4). All animals received a similar low dose for infection without specific randomization or blinding. For the SNP-strain infections, the inoculum was 34 CFU/animal. After infection,

microbiologic (Mtb growth by gastric aspirate, GA, or bronchoalveolar lavage, BAL), clinical (e.g. weight loss, cough, anorexia, activity), and immunologic (erythrocyte sedimentation rate, ESR) assessments were conducted every 2–4 weeks. Latent infection was defined at 6 months post infection in animals without clinical signs of disease, normal ESR and no evidence of Mtb growth by serial GA or BAL. Active disease was established based on evidence of clinical deterioration, persistent growth of Mtb by GA or BAL and increased ESR after 3 months post infection as previously defined [2]. In some cases, data was obtained from animals used from previously published studies[10,17]. Samples were chosen for each experiment to ensure both a broad sampling of disease states as well as an in-depth analysis of individual animals. For short-term experiments, macaques were infected for 4 weeks (n = 4) or 11 weeks (n = 3). Macaques in the barcoded Erdman strain[11] experiments were infected for 4 weeks (n = 2) (Supplemental Table 4). Animal studies were approved by the University of Pittsburgh's IACUC which followed the Public Health Service Policy on Humane Care and Use of Laboratory Animals and is AALAC approved.

Isoniazid treatment

To assess chromosomal equivalents after INH treatment among lesions for which bacteria could not be cultured, samples from previously published studies were obtained[17]. These animals had active disease and initiated treatment with INH ~13 weeks post infection.

^{18}F-PET CT imaging and analysis

Positron emission tomography (PET) using 18-fluorodeoxyglucose (18F–PET) co-registered with computed tomography (CT) was performed using a hybrid microPET Focus 220 preclinical PET scanner (Siemens Molecular Solutions, Knoxville, TN) and an 8-slice helical CT scanner (Neurologica Corp, Danvers, MA)[17]. For each specific scan, macaques were sedated, intubated and placed on a ventilator during each PET CT. For 4 week experiments, animals were scanned at baseline, 2,3 and 4 weeks after infection. PET-CT was performed only once immediately prior to necropsy in animals infected for 11 weeks and a select group of animals with active disease and latent infection. Each lung granuloma was characterized by size (mm) and metabolic activity (as measured by standard uptake volume, SUV) on each scan and lesions were tracked over time when serial scans were performed. An SUV ratio (SUVR) was developed to normalize the degree of SUV variability between scans[17]. To determine the relationship between SUVR and CFU, we used the linear regression function of Prism (GraphPad, La Jolla, CA) to determine the slope for the line of best fit including confidence intervals and goodness of fit (R^2).

Bacterial burden estimates at necropsy

PET-CT was performed 1–2 days prior to necropsy. At necropsy, scan specific lesions were prioritized for harvest and the remaining granulomas in the lung and mediastinal lymph nodes were harvested. Size of each granuloma was measured at necropsy and by pre-necropsy scan. Granulomas were dissected and one half of each was submitted for bacterial burden and the other half for histopathology as previously described[2,10]. Samples were plated on 7H10 agar supplemented with OADC and incubated for 3 weeks before enumeration of colonies. The number of bacilli per individual granuloma was determined using the CFU per gram of granuloma tissue multiplied by the weight of the granuloma, based on a standard curve of weight for granulomas of various sizes. To determine the accuracy of our standard curve, we measured CFU per granuloma using both weight and extrapolation from size for 64 granulomas from 5 randomly chosen animals. The results were highly correlative (Spearman's ρ=0.99, p<0.0001), supporting the use of size as a proxy for weight. Areas of TB pneumonia were identified grossly, harvested, weighed and a predetermined portion taken for bacterial burden estimates (measured as CFU per gram) as

previously described[2]. Granuloma histopathological characteristics were assessed by a certified primate pathologist. Specifically the granuloma type (e.g., caseous, non-necrotizing) and pattern of granulomas (focal, coalescing, disseminated) were used for analysis in these studies to determine if lesions had evidence of spreading[2]. Pairwise comparison was performed by Student's t-test for normally distributed data and non-parametric equivalent analyses were used for non-normally distributed data. Normal distribution was confirmed by D'Agostino-Pearson omnibus test. To determine statistically significant differences in CFU, groups (or animals) were compared using the Kruskal-Wallis one-way analysis of variance function in Prism with post-test pair-wise Mann-Whitney comparison of each possible pair of groups and Dunn's correction for determining significance. Percent sterilization was compared between active and latent animals, with significance determined by Student's t-test. Statistical computations were performed with Prism software (GraphPad, La Jolla, CA).

Determination of sterility

Sterile lesions were defined as lesions with no growth after 6 weeks, with a limit of detection of 10 as previously published[2]. To confirm that plates with no growth do not actually represent plates with slowly growing bacteria, we use an extended incubation time of 6 weeks. Any plate that failed to produce colonies after 6 weeks was recorded as sterile for the purposes of these analyses. We previously incubated plates for a period of one year, checking each plate at one-month intervals[2]. Only a small fraction (~1%) had new growth after 6 weeks, consistent with previous reports from resected lesions in humans[18,19]. Additionally, as a more stringent test of the potential for "dormant" or nonculturable but still potentially infectious bacilli in lesions, we analyzed data from a separate set of studies performed in our lab where latently infected macaques were administered antibody to TNF (adalimumab) to induce reactivation[10,12]. Antibody to TNF is known to be a significant trigger for reactivation in humans[20]. We previously published that TNF–specific antibody treatment for six to eight weeks resulted in reactivation of ~70% of latently infected macaques[10,12]. We reasoned that this treatment would result in regrowth of bacilli in lesions, and therefore if lesions were truly sterile, they would not grow bacilli after treatment with TNF–specific antibody. We found that 54% of the individual granulomas identified at necropsy did not grow Mtb (i.e., were sterile) among nine macaques treated with anti-TNF antibody, similar to the results reported in Fig. 3c for latent animals (58%). This stringent test provides strong evidence that these lesions do not contain viable bacilli, even under conditions of severe immunosuppression.

Creation and validation of pooled barcoded library for infection

Strains (described in Supplemental Table 1) were previously sequenced[11] and found to differ from one another by only a single nucleotide polymorphism. Individual cultures of each strain were expanded in broth culture of 7H9 supplemented with 10% Middlebrook OADC, 0.0005% tween 80, and 0.005% glycerol with shaking at 37 °C to an OD of 1.0. The inoculum for infection was prepared by mixing each strain in equal parts. To determine the potential fitness effects of each single nucleotide polymorphism, the library was expanded *in vitro* over the course of nine days, with sampling every three days.

Determination of barcoded strain identity

Two cynomolgus macaques were infected as described above with the above described barcoded library (Supplemental Table 1). At four weeks, animals were sacrificed, and individual lesions were plated for CFU. Plates were scraped, colonies were pooled, and genomic DNA was extracted as follows. Cells were harvested from plates into PBS and centrifuged at 4,000RPM for 10 minutes at 4 °C to separate the supernatant. The cell pellet

was resuspended in Tris-EDTA buffer (TE, 0.1 M Tris and 1 mM EDTA, pH 9.0). An equal volume of chloroform – methanol (2:1) was added to the cell suspension and thoroughly mixed for 5 minutes. The suspension was centrifuged again for 10 minutes at 4,000RPM at 4 °C, and both the organic and aqueous phase were discarded. After allowing the pellet to air dry for one hour, the pellet was resuspended in TE buffer and supplemented with lysozyme to final concentration of 100 μg mL^{-1}. The suspension was incubated over night at 37 °C, after which the suspension was supplemented with $1/10^{th}$ volume of 10% SDS and proteinase K to a final concentration of 100 μg mL^{-1}. After mixing by vortex, this suspension was incubated at 50 °C for 2 hours. An equal volume of phenol:chloroform (1:1) was added, and mixed well for 30 minutes before separation by centrifugation at 10,000 RPM for 15 minutes at 4 °C. The aqueous phase was removed after centrifugation and supplemented with one half volume of chloroform and again centrifuged at 14,000 RPM for 15 minutes at 4 °C. The aqueous phase was again removed and then supplemented with RNase A (Life Technologies) to a final concentration of 25 μg mL^{-1} and incubated at 37 °C for one hour. The samples were then stored at 4 °C for 10 minutes, before being supplemented with an equal volume of phenol:chloroform, and again centrifuged at 14,000RPM for 15 minutes at 4 °C. The aqueous layer was again removed and supplemented with one-half volume of chloroform, after which samples were centrifuged at 14,000 RPM for 15 minutes at 4 °C, and the aqueous layer was removed. DNA was precipitated from the aqueous layer by adding one volume of isopropanol and incubating at −20 °C for 12 hours. Mtb genomic DNA was washed using 70% ethanol, and dissolved in sterile distilled deionized water.

Each sample was used as template for eight PCR reactions (Supplemental Table 5) to amplify the eight loci listed in Supplemental Table 1. Each primer pair contained a sequence tag from which a second PCR reaction was initiated using an additional set of primers to attach the sequence content necessary for Illumina sequencing and barcoding (Supplemental Table 5). Pooled libraries were subsequently sequenced using an Illumina GenomeAnalyzer IIx, with a read length of 54 bp. A mean of 840,000 reads was collected per sample. The reads were aligned to the eight targeted loci, yielding approximately 100,000 reads covering each polymorphic site. The frequency of each allele was calculated based on the proportion of nucleotides observed. To distinguish between background signal and noise resulting from both sequencing and experimental variation, we required a percentage greater than 2.5. Strain counts were determined for each sample, and the relationship to $\log_{10}$(CFU) per granuloma was determined by linear regression, Spearman correlation, and comparison between groups (where groups were samples with *x* strains) by Kruskal-Wallis one-way analysis of variance. All tests were performed using Prism (GraphPad, La Jolla, CA).

Determining Barcode prevalence and fitness *in vivo*

To determine the probability of observing any given barcode at the end of infection, we generated a stochastic simulation of sampling from the inoculum stock. To simulate the sample, we ran one million random simulations, where the number of each barcode was determined by a random number (X_i), where X_i is a binomial random variable: $X_i \sim B(34, S_i)$. S_i, the probability of success of each trial, was estimated based on the prevalence of each barcode in the inoculum stock and the number of trials (34) was estimated by a plating of the inoculum, but the sum of X_i varies stochastically with each sampling. To determine if the prevalence post-infection differed significantly from the prevalence before infection, the number of runs in which the simulated sampling exceeded the prevalence post infection was divided by the total number of runs (one million). Significant deviations from the inoculum were defined as those occurring in less than 5% of runs, suggesting this observation was unlikely to occur by chance. Notably, we did not correct for repeated testing of each barcode ($n = 8$), leading us to conservatively "over call" strains that significantly deviated from the

inoculum. Barcode I3 is the only isolate whose prevalence was significantly unlikely by chance, where $p = 0.023$. We reasoned that fitness changes could explain this result. To better understand the fitness change necessary to skew the observed distribution of barcodes after 28 days of growth, we expanded our simulation. The prevalence of each barcode after 28 days of infection was determined by:

$$pr(i_{t28}) = \frac{N_{i0} * e^{f*r*t}}{N_{total}} \quad (1)$$

where $pr(i_{t28})$ is the prevalence of each barcode (i) after 28 days of infection based on the initial population (simulated previously by random sampling) times the exponential growth equation. The rate parameter (r) of the exponential growth equation was parameterized based on estimates determined by CEQ (detailed below), and time (t) was determined based on length of infection (28 days). Fitness (f) was iterated from a no change in fitness (f = 1.00) to 15% (f = 1.15) by an interval of 1% (0.01) for barcode I3 only. For all other barcodes, f = 1.00. To determine the fitness level at which the probability of the observed prevalence of strain I3 was greater than 5%, the number of runs in which the simulated growth exceeded the prevalence post infection was divided by the total number of runs (one million) for each fitness iteration.

Isolation and quantification of Mtb genomes from lesions

Following necropsy, samples were stored in PBS at −80 °C until processing. Investigators were blinded as to the clinical status of each sample. Volumes were tracked throughout genomic extraction to correct for volume loss. Samples were resuspended in 1 mL Tris-EDTA buffer, pH 8.0, and supplemented with 300 uL of 70 °C phenol-chloroform-isoamyl alcohol (25:24:1, Sigma-Aldrich). Samples were mixed by inversion and incubated at room temperature for 10 minutes before being transferred to tubes containing 250uL of 0.1 mm zirconia-silica beads (MP Biomedicals) and pulsed twice for 30 seconds each using the FastPrep 24 system (MP Biomedicals), with a fiveminute break between pulses. The supernatant was then separated by centrifugation at 14,000 RPM, and supplemented with 50uL of 5 M sodium chloride. The phenol-chloroform-isoamyl alcohol (25:24:1, Sigma-Aldrich) extraction was repeated and samples were again centrifuged at 14,000 RPM to separate the aqueous phase. Genomic DNA was precipitated using one volume of isopropanol and one-tenth volume of 3 M sodium acetate (pH 5.2) and washed with one volume of 70% ethanol. A subset of samples was further purified by dialysis. Mtb genomic DNA was then quantified using the previously described primer-probe combination[13] (Supplemental Table 5) (Integrated DNA Technologies). Chromosomal equivalents (CEQ) were quantified in relation to a standard curve derived from serial dilution of Mtb genomic prepared from liquid culture. Real time quantitative PCR was performed in triplicate on the Viia 7 (Life Technologies) using TaqMan Universal Master Mix II (Life Technologies). Researchers conducting sample processing and quantification of CEQ were blinded to the live bacterial counts until the time of analysis. To determine statistically significant differences in CEQ, groups were compared using the Kruskal-Wallis one-way analysis of variance function in Prism (GraphPad, La Jolla, CA) with post-test pair-wise Mann-Whitney comparison of each possible pair of groups and Dunn's correction for determining significance. To determine correlates between time, CFU/CEQ, and histopathological characteristic of each lesion, these data were correlated using the "corrcoef" function in Matlab (Natick, MA) and plotted according strength of correlation. CFU/CEQ were log normalized before analysis.

Mathematical model of population dynamics and estimates of replication rate

To determine the rate of growth and death of the Mtb population in individual lesions, we developed a set of ordinary differential logistic equations describing population dynamics (equations 1 & 2) in each lesion. To accurately describe both the expansion of the viable bacterial population (CFU) and the decline of the viable bacterial population following the onset of adaptive immunity after four weeks, these data were divided into two separate phases (I & II) and analyzed by the following equations (2 & 3 respectively). The total bacterial population (represented by chromosomal equivalents, CEQ) was modeled by equation (2) only:

$$\frac{dN_1}{dt}=(r_1*N_1)*\frac{(K_1-N_1)}{K_1} \quad (2)$$

$$\frac{dN_2}{dt}=(r_2*N_2)*\frac{(N_2-K_2)}{K_2} \quad (3)$$

Here, r represents the growth rate of the population in replications per day, N_1 and N_2 represent the population size, and K represents carrying capacity. The parameters for equations (2) & (3) were optimized to best fit the medians for CEQ and CFU at each time point where data were available using Matlab (Natick, MA). Specifically, scripts were created to fit the equations above using the *nlinfit* function with maximum iterations set to 10,000 and the weight function for robust fitting set to “fair”. The initial values were chosen based on estimates derived from the data, and adjusted to provide the fit and final parameter estimates that produced the smallest residuals. To determine the replication rate (in days per duplication), we began with the discrete form of the logistic equation:

$$x_t=x_0*(1+r^*\frac{K_{CEQ}-fit_{CEQ}(t)}{K_{CEQ}})^t \quad (4)$$

By setting x_t equal to 2^*x_0, and solving for t, we derived the time required for the population to double, t_d.

$$t_d=\log(2)/\log(1+r_{CEQ}*\frac{K_{CEQ}-fit_{CEQ}(t)}{K_{CEQ}}) \quad (5)$$

Where t_d represents the time for the population to double, r_{CEQ} is the estimate of r_1 derived by fitting equation (2) to the median CEQ for each time point, K_{CEQ} is the estimate of K_1 derived by fitting equation (2) to the median CEQ for each time point, and $fit_{CEQ}(t)$ is the modeled population size of CEQ derived from equation (2). Equation (5) was used to determine both average and instantaneous doubling times, where instantaneous doubling times where estimated for each time point from $t(1)$ to $t(600)$, and average doubling time for a given time point was estimated by summing across all previous instantaneous doubling times and dividing by the total time elapsed. For estimates of doubling after fit_{CEQ} exceeds K_{CEQ}, K_{CEQ} was set as the maximum value for fit_{CEQ}; the modeled value of fit_{CEQ} actually fluctuate slightly around K_{CEQ} consistent with logistic models of population growth. As instantaneous estimates of slope fail to capture the stable nature of population size, K_{CEQ} was substituted for these time points. Notably, the estimates of population growth derived from equation (2) parameterized by CEQ data were used to derive doubling times, which are applicable to the viable population (CFU).

Supplementary Material

Refer to Web version on PubMed Central for supplementary material.

Acknowledgments

These studies were funded by the Bill and Melinda Gates Foundation (grants to JLF and PLL), Otis Childs Trust/ Children's Hospital of Pittsburgh Foundation (PLL), US National Institute of Health, National Institute of Allergy and Infectious Diseases DAIT BAA-05–10 (JLF), US National Institute of Health HL106804 (JLF), US National Institute of Health AI094745 (JLF), US National Institute of Health DP2 0D001378 (SMF), US National Institute of Health AI076217 (SMF), the Howard Hughes Medical Institute, Physician Scientist Early Career Award (SMF), the Harvard Merit Fellowship (CBF), the Burroughs Wellcome Foundation Investigator in the Pathogenesis of Infectious Diseases Fellowship (SMF), the Robert A. Welch Foundation (JS) and the Melvin J. and Geraldine L. Glimcher Associate Professorship (SMF). We are grateful to E. Klein and C. Janssen for necropsies, C. Scanga for coordination of studies, M. Rodgers, C. Cochran and C. Bigbee for excellent technical assistance and M. O'Malley, P. Johnston, J. Tomko, D. Fillmore, J. Frye for outstanding veterinary technical assistance, the members of the Flynn and Fortune labs for helpful discussions, and to B. Bloom, D. Young, and E. Rubin for helpful comments on the manuscript.

References

1. Zumla A, Raviglione M, Hafner R, von Reyn CF. Tuberculosis. N Engl J Med. 2013; 368:745–755. [PubMed: 23425167]
2. Lin PL, et al. Quantitative comparison of active and latent tuberculosis in the cynomolgus macaque model. Infect Immun. 2009; 77:4631–4642. [PubMed: 19620341]
3. Capuano SV 3rd, et al. Experimental Mycobacterium tuberculosis infection of cynomolgus macaques closely resembles the various manifestations of human M. tuberculosis infection. Infect Immun. 2003; 71:5831–5844. [PubMed: 14500505]
4. Barry CE 3rd, et al. The spectrum of latent tuberculosis: rethinking the biology and intervention strategies. Nat Rev Microbiol. 2009; 7:845–855. [PubMed: 19855401]
5. Lin PL, Flynn JL. Understanding latent tuberculosis: a moving target. J Immunol. 2010; 185:15–22. [PubMed: 20562268]
6. Kaplan G, et al. Mycobacterium tuberculosis growth at the cavity surface: a microenvironment with failed immunity. Infection and immunity. 2003; 71:7099–7108. [PubMed: 14638800]
7. Via LE, et al. Infection dynamics and response to chemotherapy in a rabbit model of tuberculosis using [(1)(8)F]2-fluoro-deoxy-D-glucose positron emission tomography and computed tomography. Antimicrob Agents Chemother. 2012; 56:4391–4402. [PubMed: 22687508]
8. Davis JM, Ramakrishnan L. The role of the granuloma in expansion and dissemination of early tuberculous infection. Cell. 2009; 136:37–49. [PubMed: 19135887]
9. Canetti, G. The Tubercle Bacillus. New York, NY: Springer Publishing Co, Inc; 1955.
10. Lin PL, et al. Metronidazole prevents reactivation of latent Mycobacterium tuberculosis infection in macaques. Proc Natl Acad Sci U S A. 2012; 109:14188–14193. [PubMed: 22826237]
11. Ford CB, et al. Use of whole genome sequencing to estimate the mutation rate of Mycobacterium tuberculosis during latent infection. Nat Genet. 2011; 43:482–486. [PubMed: 21516081]
12. Lin PL, et al. Tumor necrosis factor neutralization results in disseminated disease in acute and latent Mycobacterium tuberculosis infection with normal granuloma structure in a cynomolgus macaque model. Arthritis Rheum. 2010; 62:340–350. [PubMed: 20112395]
13. Munoz-Elias EJ, et al. Replication dynamics of Mycobacterium tuberculosis in chronically infected mice. Infection and immunity. 2005; 73:546–551. [PubMed: 15618194]
14. Wallis RS, et al. Tuberculosis biomarkers discovery: developments, needs, and challenges. Lancet Infect Dis. 2013; 13:362–372. [PubMed: 23531389]
15. Walzl G, Ronacher K, Hanekom W, Scriba TJ, Zumla A. Immunological biomarkers of tuberculosis. Nat Rev Immunol. 2011; 11:343–354. [PubMed: 21475309]
16. Lin PL, et al. Early events in Mycobacterium tuberculosis infection in cynomolgus macaques. Infection and immunity. 2006; 74:3790–3803. [PubMed: 16790751]

Online References

17. Lin PL, et al. Radiologic responses in cynomolgus macaques fro assessing tuberculosis chemotherapy regimens. Submitted for publication. 2013
18. Kennedy HE, Vandiviere HM, Willis HS. The effects of extended incubation on propagability of tubercle bacilli. Am Rev Tuberc. 1958; 77:802–814. [PubMed: 13533799]
19. Vandiviere HM, Loring WE, Melvin I, Willis S. The treated pulmonary lesion and its tubercle bacillus. II. The death and resurrection. Am J Med Sci. 1956; 232:30–37. passim. [PubMed: 13326887]
20. Keane J, et al. Tuberculosis associated with infliximab, a tumor necrosis factor alpha-neutralizing agent. N Engl J Med. 2001; 345:1098–1104. [PubMed: 11596589]

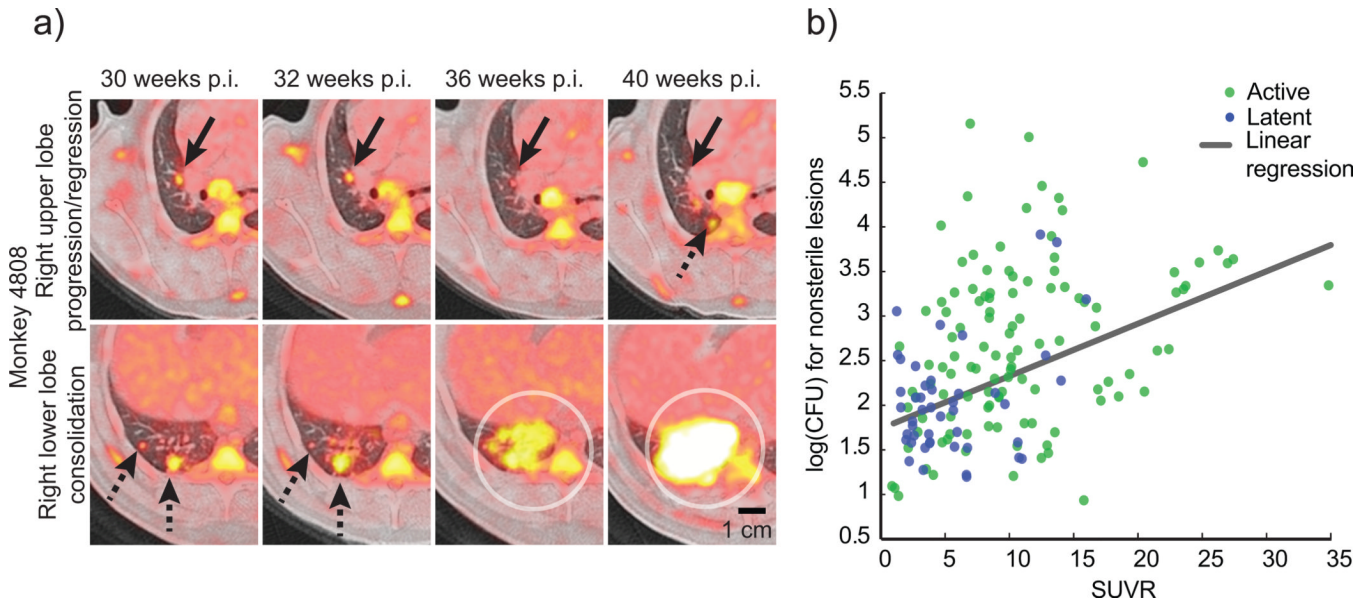

Figure 1. Serial imaging reveals the dynamic evolution of lesions in TB

(**a**) A PET/CT image of progressing and regressing lesions is shown from the same animal that developed active disease following low dose infection. Serial PET/CTs reveal a resolving lesion in the right upper lobe (upper panel, solid black arrows) at the same time that new lesions appear (dashed black arrow). In the right lower lobe (lower panel), lesions progress (dashed black arrows) and new lesions coalesce to form a consolidation (circles). (**b**) 18-FDG avidity (SUVR) is positively correlated with bacterial numbers in lesions (Spearman's • = 0.4431), though there is considerable variability in both. A linear regression model of SUVR vs. CFU reveals significant predictive value (slope = 0.05847 +/− 0.009730, $p < 0.001$). Symbols represent individual lesions ($n = 274$) from active (green, $n = 15$) or latent (blue, $n = 10$) monkeys.

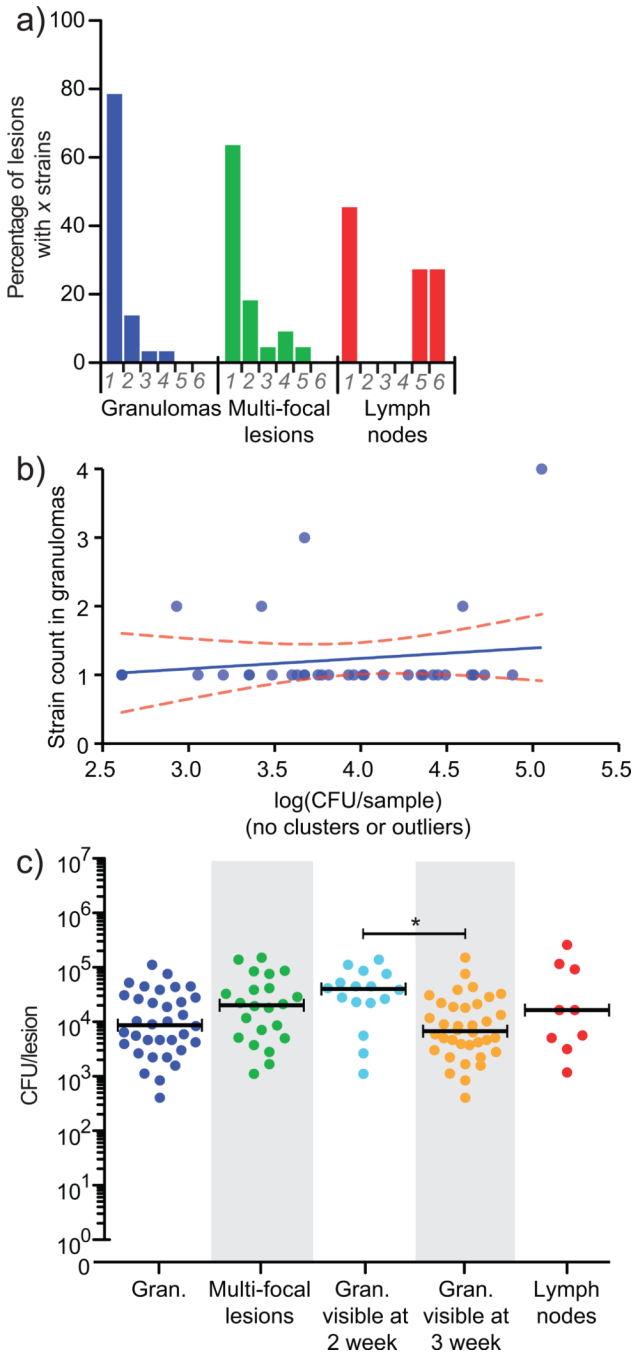

Figure 2. The majority of lesions in monkeys are initiated by a single bacterium

(**a**) 79% of granulomas (n = 37) contained a single barcode, although all eight barcodes were represented in each animal. When multi-focal lesions (lesions with histologic evidence of being comprised of two or more granulomas, n = 22) were analyzed separately, many (64%) contained only a single barcode, suggesting these lesions arose through localized spreading as opposed to coalescence of nearby lesions. In contrast, thoracic lymph nodes contained as many as six barcodes (n = 13), reflecting draining of infecting bacilli from lungs to lymph nodes. Bacterial load was similar in these two animals to the four other animals analyzed at 4 weeks post-infection (Supplemental Figure 1b). (**b**) A linear regression of total bacterial

load in individual granulomas (n=37) indicates no relationship between CFU and the number of barcodes recovered, such that initial bacterial load did not influence later bacterial load (Spearman's • = 0.2404, slope = 0.1510 +/− 0.1919, $p = 0.4372$, Kruskal-Wallis, $p = 0.1120$). (**c**) A range of bacterial load per lesion is present in individual lesions, in clustered lesions, and lymph nodes. Bacterial load in lesions visible at 2 weeks p.i. by PET-CT ($n = 16$) is significantly higher than those not visible until 3 weeks ($n = 36$, $p < 0.05$), with substantial overlap, suggesting that the timing of lesion formation can affect bacterial burden. Bars represent medians.

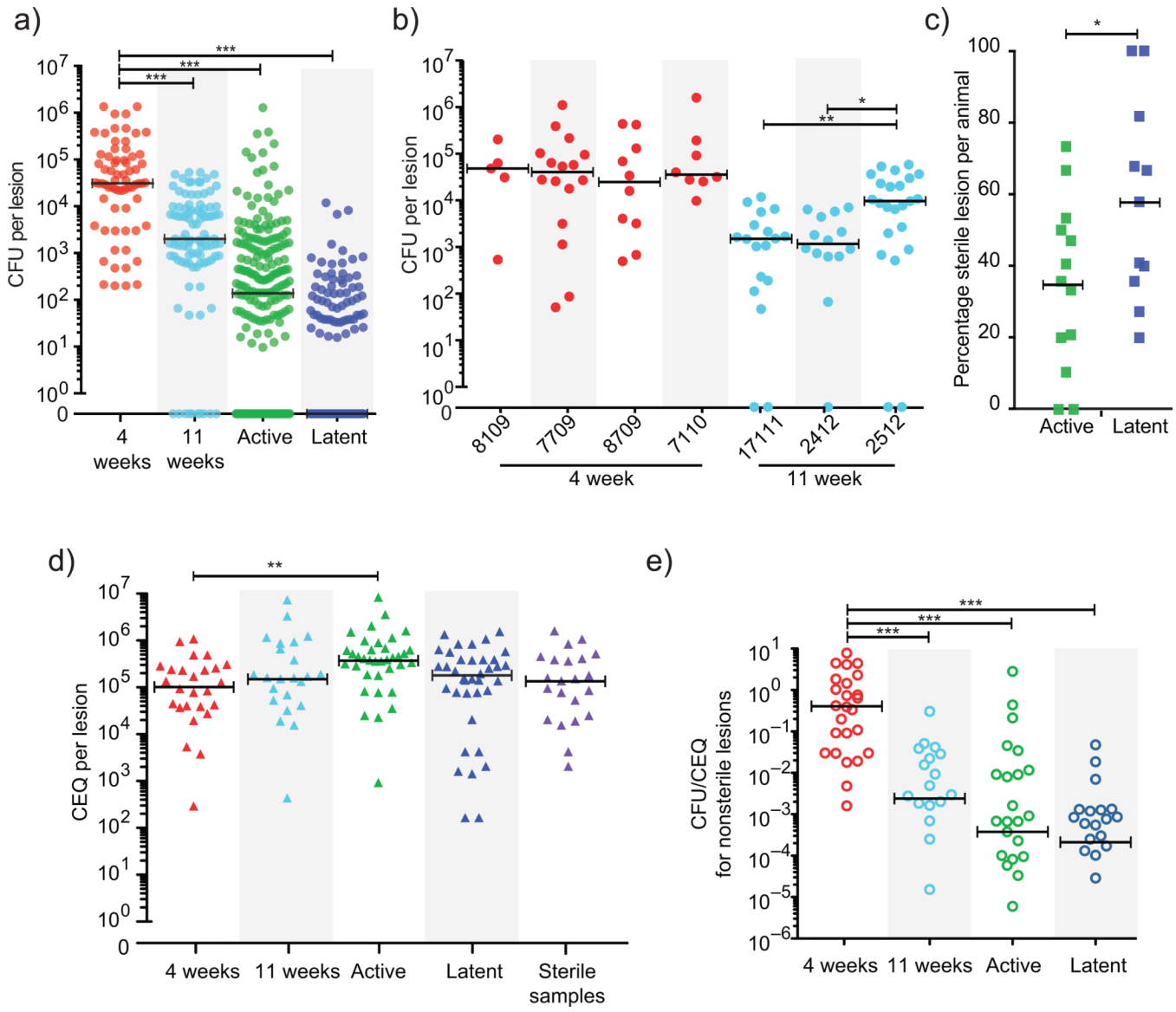

Figure 3. CFU and CEQ reflect viable and total bacterial burden in individual lesions

(**a**) CFU in lesions from monkeys at 4 weeks (4 animals, 68 lesions) is significantly higher than at 11 weeks (3 animals, 98 lesions), in active disease (13 animals, 222 lesions) and in clinically latent infection (11 animals, 145 lesions) ($p < 0.001$). All groups are significantly different by pairwise comparison ($p < 0.001$). Circles represent individual lesions. The median for latent animals is zero. (**b**) Individual monkeys necropsied at 4 weeks and 11 weeks are shown; circles represent individual lesions. By 11 weeks, there are significant differences between animals ($p < 0.05$). (**c**) The percentage of sterile lesions in monkeys with latent infection ($n = 11$) is significantly higher than in monkeys with active disease ($n = 13$, $p < 0.05$); however in both conditions the majority of animals contain sterile lesions. Squares represent individual animals. (**d**) CEQ per lesion is similar across all categories ($n = 26$ for 4 week, $n = 23$ for 11 week, $n = 36$ for active, $n = 37$ for latent). CEQ from lesions of active monkeys was significantly higher compared to 4 weeks p.i. reflecting additional replication. CEQ is also similar in sterile lesions ($n = 22$), supporting the observation that CEQ are stable in the absence of replication. Triangles represent individual lesions. (**e**) The

ratio of CFU to CEQ in individual non-sterile lesions drops significantly after 4 weeks (n = 26), indicating bacterial killing over time (n = 22 for 11 week animals, n = 29 for active, n = 28 for latent), coincident with the onset of the adaptive immune response[16] ($p < 0.001$). Open circles represent individual lesions. For all panels, *$p < 0.05$, **$p < 0.01$,***$p < 0.001$, statistical tests as indicated in **Methods**, bars represent medians.

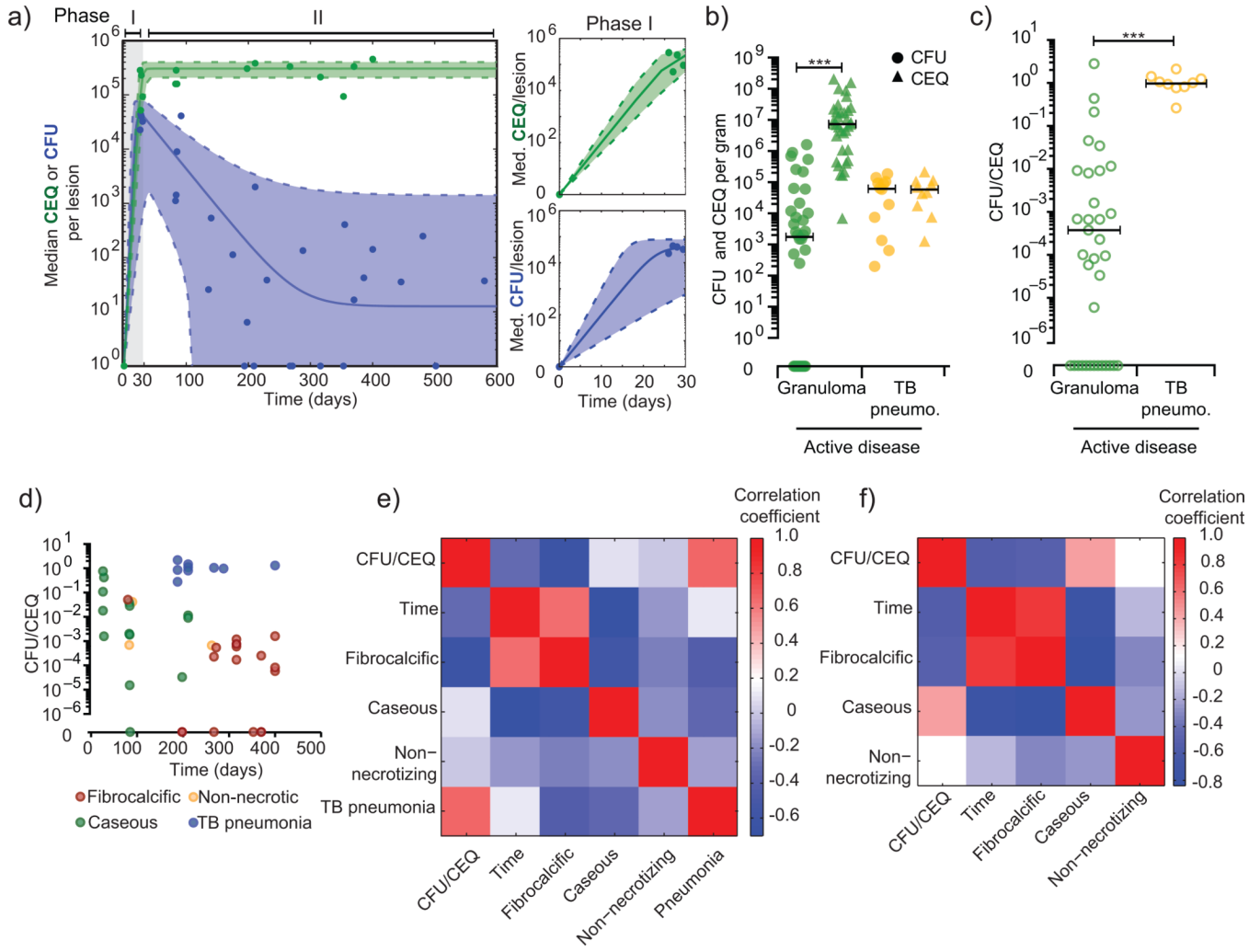

Figure 4. Models and correlates of replication and killing

(**a**) Median CEQ (green) and CFU (blue) were fit with ordinary differential equations describing growth and death in individual lesions. t_0 data were inferred from our barcode data suggesting most granulomas start with a single bacterium. CFU data were modeled as two phases – phase I represents initial growth (t = 0:30 days); phase II represents a subsequent killing (t = 30:600 days). Doubling times in individual lesions were inferred from CEQ and CFU fitted curves (Supplemental Table 3). Phase I is shown in detail in panels on the right, and validated against 3 week CFU samples in Supplemental Figure 3. (**b**) CFU (circles) and CEQ (triangles) per gram of tissue are shown for granulomas from active disease animals or sites with TB pneumonia. (**c**) The ratio of CFU/gm to CEQ/gm in TB pneumonia samples suggests reduced killing at these sites. (**d**) Plotting time, histopathology, and CFU/CEQ reveals associations between these variables. (**e**) A correlation matrix reveals that the characteristics *TB pneumonia* (r = 0.66, p = 9.24E-07) and *fibrocalcific* (r = −0.62, p = 6.95E-06) are significantly correlated with CFU/CEQ, though to opposite effect. TB pneumonia is positively correlated with CFU/CEQ (i.e. little killing), and poorly correlated with time. Both fibrocalcific and caseous lesions are correlated with time p.i. (**f**) We removed TB pneumonia samples from the analysis to focus on granulomatous sites. Time is significantly correlated with CFU/CEQ (r = −0.53, p = 0.001),

suggesting that killing increases over time in these lesions and the dominant histopathology switches from caseous to fibrocalcific.